Synchronization Tomography: A Method for Three-Dimensional Localization of Phase Synchronized Neuronal Populations in the Human Brain using Magnetoencephalography

P. A. Tass,[1,2] T. Fieseler,[1] J. Dammers,[1] K. Dolan,[1] P. Morosan,[1] M. Majtanik,[1] F. Boers,[1] A. Muren,[1] K. Zilles,[1,3] and G. R. Fink[1,4]

[1]*Institute of Medicine, Research Center Jülich, 52425 Jülich, Germany*
[2]*Department of Stereotaxic and Functional Neurosurgery, University Hospital, 50924 Cologne, Germany*
[3]*C. and O. Vogt Institute for Brain Research, Heinrich Heine University, 40225 Düsseldorf, Germany*
[4]*Department of Neurology, University Hospital RWTH, 52074 Aachen, Germany*

We present a noninvasive technique which allows the anatomical localization of phase synchronized neuronal populations in the human brain with magnetoencephalography. We study phase synchronization between the reconstructed current source density (CSD) of different brain areas as well as between the CSD and muscular activity. We asked four subjects to tap their fingers in synchrony with a rhythmic tone, and to continue tapping at the same rate after the tone was switched off. The phase synchronization behavior of brain areas relevant for movement coordination, inner voice, and time estimation changes drastically when the transition to internal pacing occurs, while their averaged amplitudes remain unchanged. Information of this kind cannot be derived with standard neuroimaging techniques like functional magnetic resonance imaging or positron emission tomography.

Phase synchronization occurs in periodic [1,2] and chaotic oscillators [3], and has been found in various physical [4] and biological [5,6] systems. In animals, phase synchronization has been demonstrated to be a fundamental mechanism for motor control [7]. Active neuronal populations in the brain generate currents which, in turn, produce a magnetic field that can non-invasively be measured by means of magnetoencephalography (MEG) with a time resolution in the millisecond range. Phase synchronization can be detected in noisy, nonstationary MEG signals [5]. However, the spatial resolution of this approach has so far been severely limited, since MEG sensors measure the magnetic field which may originate from different brain areas. To study normal brain function as well as pathological synchronization (e.g., in Parkinson's disease and epilepsy) a correct anatomical localization of synchronization processes is crucial. We here present a novel method which allows a reliable 3D localization of phase synchronization in the human brain with MEG.

We first reconstructed the cerebral current source density $\mathbf{j}(\mathbf{x}, t)$, which generates the measured magnetic field, in each volume element (voxel) for all times t with magnetic field tomography [8]. $\mathbf{x}$ denotes the spatial coordinates representing the center of a voxel. We then analyzed phase synchronization voxel by voxel: To detect *cerebro-muscular synchronization* (CMS) we determined phase synchronization between the muscular activity recorded with electromyography (EMG) and $\mathbf{j}(\mathbf{x}, t)$ in each of the voxels representing the brain. To detect *cerebro-cerebral synchronization* (CCS) we determined phase synchronization of $\mathbf{j}(\mathbf{x}, t)$ in all pairs of voxels.

We applied our approach to study internal rhythm generation in humans. The latter is essential for performing rhythmic movements without external stimulus, e.g., during locomotion or skilled actions like playing muscial instruments. We performed a paced finger tapping (PFT) experiment [9], where subjects are first asked to tap with their index finger in synchrony with a periodic train of tones (external pacing). After discontinuing the tones, the subjects then have to continue the tapping at the same pace (internal pacing), by generating the rhythm alone.

Behavioral studies of movement timing in PFT studies revealed an internal timekeeping system which appears to be independent of feedback mechanisms [9], and which is severely impaired after cerebellar damage [10] or in Parkinson's disease [11]. Brain areas active during PFT were localized with functional magnetic resonance imaging (fMRI), which detects neuronal activity indirectly by measuring an increase of the blood oxygenation level [12]. However, as yet, synchronization processes could not be investigated because of the limited time resolution of fMRI. In contrast, by applying our synchronization tomography to MEG signals recorded during a PFT experiment, we reveal that both CMS and CCS are remarkably different during external vs internal pacing. We show that the synchronization behavior of relevant brain areas changes drastically when the transition to internal pacing occurs, while their activation (i.e., averaged amplitude) is similar under both conditions.

We recall how to detect $n{:}m$ phase synchronization in noisy nonstationary scalar signals s_1 and s_2 [5]: We compute the instantaneous phase ϕ_j of s_j with the Hilbert transform [13] and introduce the cyclic relative

phase $\Psi_{n,m}(t) = \varphi_{n,m}(t) \bmod 1$, where $\varphi_{n,m}(t) = [n\phi_1(t) - m\phi_2(t)]/(2\pi)$ is the normalized $n{:}m$ phase difference. Phase synchronization is characterized by the appearance of peaks in the distribution of $\Psi_{n,m}$ [1,3] and quantified by comparing the actual distribution of $\Psi_{n,m}$ with a uniform one [5]: As the data are nonstationary, we perform a sliding window analysis and determine $\tilde{\rho}_{n,m}[s_1(t), s_2(t)]$, the $n{:}m$ synchronization index of s_1 and s_2 evaluated in the window $W(t) = [t - T/2, t + T/2]$ according to $\tilde{\rho}_{n,m}[s_1(t), s_2(t)] = [S_{\max} - S(t)]/S_{\max}$, where $S(t) = -\sum_{k=1}^{N} p_k \ln p_k$ is the entropy of the distribution of $\Psi_{n,m}$ in $W(t)$, and p_k denotes the relative frequency of finding $\Psi_{n,m}$ within the kth bin. $S_{\max} = \ln N$, where N is the optimal number of bins [13]. $0 \le \tilde{\rho}_{nm}[s_1(t), s_2(t)] \le 1$ holds for all t, where $\tilde{\rho}_{nm} = 0$ corresponds to a uniform distribution (no synchronization) and $\tilde{\rho}_{nm} = 1$ to a Dirac-like distribution (perfect synchronization).

The *synchronization index between a scalar signal* $s(t)$ (like the electromyographically recorded muscular activity) *and a vector signal* $\mathbf{j}(\mathbf{x}, t) = [j_1(\mathbf{x}, t), j_2(\mathbf{x}, t), j_3(\mathbf{x}, t)]$(with fixed $\mathbf{x}$) is

$$\tilde{\rho}_{n,m}[s(t), \mathbf{j}(\mathbf{x}, t)] = \max_{k=1}^{3} \tilde{\rho}_{n,m}[s(t), j_k(\mathbf{x}, t)]. \qquad (1)$$

This definition reduces the impact of the coordinate system's orientation on the synchronization index. In contrast, $\tilde{\rho}_{n,m}[s(t), \mathbf{j}(\mathbf{x}, t)] = \{\sum_{k=1}^{3} \tilde{\rho}_{n,m}[s(t), j_k(\mathbf{x}, t)]^2/3\}^{1/2}$ would be "artificially" small, when one or two coordinates of $\mathbf{j}$ vanish due to the orientation of the coordinate system. Analogously, the *synchronization index between two vector signals*, the currents $\mathbf{j}(\mathbf{x}_1, t)$ and $\mathbf{j}(\mathbf{x}_2, t)$(with fixed $\mathbf{x}_1$ and $\mathbf{x}_2$), reads

$$\tilde{\rho}_{n,m}[\mathbf{j}(\mathbf{x}_1, t), \mathbf{j}(\mathbf{x}_2, t)] = \max_{l=1}^{3} \tilde{\rho}_{n,m}[j_l(\mathbf{x}_1, t), \mathbf{j}(\mathbf{x}_2, t)]. \quad (2)$$

We performed MEG and EMG measurements during a PFT experiment in four healthy male subjects. During the first minute the subjects had to tap with their right index finger in synchrony with an external cue administered at 2 Hz (external pacing). During the second minute the external pacing was terminated, and the subjects had to continue the tapping with the same rate as during the first minute (internal pacing). We registered the EMG from two antagonistic muscles, the right flexor digitorum muscle (RFM) and the right extensor indices muscle. $\mathbf{j}(\mathbf{x}, t)$ and the EMG signal were filtered with a bandpass corresponding to the main EMG frequency component (1–3 Hz, denoted as *2-Hz band* below, Fig. 1). Subjects were able to maintain the 2-Hz tapping after discontinuing the tones [Fig. 1(c)]. Apart from the frequency peak in the 2-Hz band, in several brain areas $\mathbf{j}(\mathbf{x}, t)$ also displayed a peak in the 3–5 Hz range (denoted as *4-Hz band*) (Fig. 1). Hence, $\mathbf{j}(\mathbf{x}, t)$ was additionally filtered with a bandpass extracting the 4-Hz band (Fig. 1) [14]. To avoid spurious detection of synchronization, we prepare surrogates by replacing $s(t)$ and $j_k(\mathbf{x}, t)$ by white noise signals $u(t)$ and $v_k(\mathbf{x}, t)$ filtered with the same bandpass as
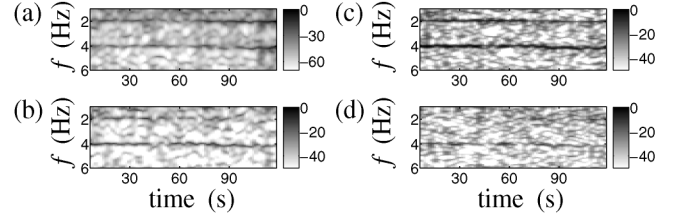
FIG. 1. Time-dependent power spectral density in dB (a) of an original MEG signal from a channel over the left sensorimotor cortex (SMC), (b) of the strongest component of the cerebral current source density $\mathbf{j}$ from SMC, (c) of the preprocessed EMG signal of the right flexor digitorum muscle after standard preprocessing, i.e., high-pass filtering (> 30 Hz) followed by rectification (where $x \to |x|$), applied to extract the burst activity, and (d) of the strongest component of $\mathbf{j}$ from the secondary auditory cortex. Yule-Walker algorithm [13] with window length $= 12$ s, step size $= 1.3$ s.

used for the original signals [5]. The 99th percentiles of the distributions of $\tilde{\rho}_{n,m}[u(t), v_k(\mathbf{x}, t)]$ and $\tilde{\rho}_{n,m}[v_l(\mathbf{x}_1, t), v_k(\mathbf{x}_2, t)]$ serve as confidence levels $\rho_{n,m}^{A}$ and $\rho_{n,m}^{B}$ which are subtracted from (1) and (2) [16].

Additionally we study the amplitude dynamics of $\mathbf{j}(\mathbf{x}, t)$ in all areas engaged in CMS or CCS processes. For each voxel with nonvanishing synchronization indices (1) and (2) we filter $j_k(\mathbf{x}, t)$ with the same bandpass filters as used for the CCS or CMS analysis. The Hilbert transform [13] yields $A_k(\mathbf{x}, t)$, the instantaneous amplitude of the bandpass filtered $j_k(\mathbf{x}, t)$. The *averaged amplitude*

$$\bar{A}(\mathbf{x}, t) = \frac{1}{T} \int_{t-T/2}^{t+T/2} \left[\sum_{k=1}^{3} A_k^2(\mathbf{x}, \xi) \right]^{1/2} d\xi \qquad (3)$$

of $\mathbf{j}(\mathbf{x}, t)$ is obtained by averaging over the same window $W(t) = [t - T/2, t + T/2]$ as used for (1) and (2) [14].

To rule out spurious synchronization introduced by the inverse technique [8], we have tested our approach in detail with simulated data. For this, the x coordinate ξ_1 of a Rössler system [15] serves as time course of a current with time-independent orientation and location $\mathbf{x}_0$ in the left sensorimotor cortex (SMC) of a real brain: $\mathbf{j}(\mathbf{x}_0, t) = \mathbf{h}\xi_1(t)$, $\mathbf{j}(\mathbf{x}, t) = 0$ for $\mathbf{x} \ne \mathbf{x}_0$. For each time t we calculate the corresponding magnetic field. To model machine noise, to each MEG signal we add Gaussian white noise (delta-correlated in time, uncorrelated between sensors). For these simulated signals we compute $\tilde{\rho}_{n,m}$ from Eq. (1) between ξ_1 and all voxels. For a wide range (from 0.1 to 10) of the signal-to-noise ratio between artificial magnetic field and machine noise our method robustly localizes the area of strongest synchronization with ξ_1 close to $\mathbf{x}_0$ [Fig. 2(a)]. The synchronization tomography works comparably well in case of two or three coupled Rössler systems serving as sources for the magnetic field.

In Figs. 1–3 we demonstrate the results of one of the subjects, since all subjects showed consistent results. Strong 1:1 or 1:2 synchronization between muscular

activity and brain currents is found in the left premotor cortex (PMC), left SMC (consisting of primary motor and primary sensory cortex), left secondary auditory cortex (AC), right secondary auditory cortex (not shown in Fig. 2), and left cerebellum (LC) (Fig. 2) [14]. Neither within nor between these areas do we find 2:1 phase synchronization between the 2-Hz and the 4-Hz bands. This indicates that the 4-Hz band is not just a harmonic of the 2-Hz band, but a functionally separate oscillation [2]. Accordingly, the time dependent synchronization behavior of the 2-Hz and the 4-Hz bands is different [Figs. 3(d)–3(f)].

Only one synchronization process, namely 1:1 CMS between RFM and SMC, strongly decreases after discontinuing the tones, while 1:2 CMS between RFM and SMC remains strong throughout the experiment [Fig. 3(d)]. The 1:2 CMS between RFM and SMC observed here might be sufficient for realizing the maintained alternating muscular action, while the 1:1 CMS between RFM and SMC might be a correlate of a strong proprioceptive feedback [17]. In contrast, all other synchronization processes are particularly strong during internal pacing: (i) 1:1 CMS between RFM and LC (where the right cerebellum is responsible for pure sensorimotor processing for the right finger) [Fig. 3(e)], (ii) synchronization between AC and muscular activity and between AC and SMC as well as between AC and PMC [not shown, all similar to Fig. 3(f)], (iii) 1:1 CCS between SMC and PMC [Fig. 3(f)]. Thus, an increase of synchronization (both CCS and CMS) involving areas relevant for time estimation (LC), movement coordination (PMC, LC), and inner voice (AC) [18] appears to be the correlate of an internal clock during internal pacing.

Our approach is superior to linear coherence, the standard tool in neuroscience for the study of synchronization: (a) Coherence is not equivalent to phase synchronization, and oscillators may have coherent signals without being phase synchronized [3,5,19]. In particular, linear coherence cannot distinguish between phase synchronization and linear superposition [19]. Consequently, coherence leads to a distinct spatial overestimation of CMS and CCS processes (not shown due to space constraints). (b) Coherence is not able to distinguish between different types of $n:m$ synchronization. In contrast, we found that even within a single brain area a 2-Hz and a 4-Hz rhythm may coexist which are functionally separate (i.e., the two are not 1:2 synchronized), and which behave completely different concerning their 1:1
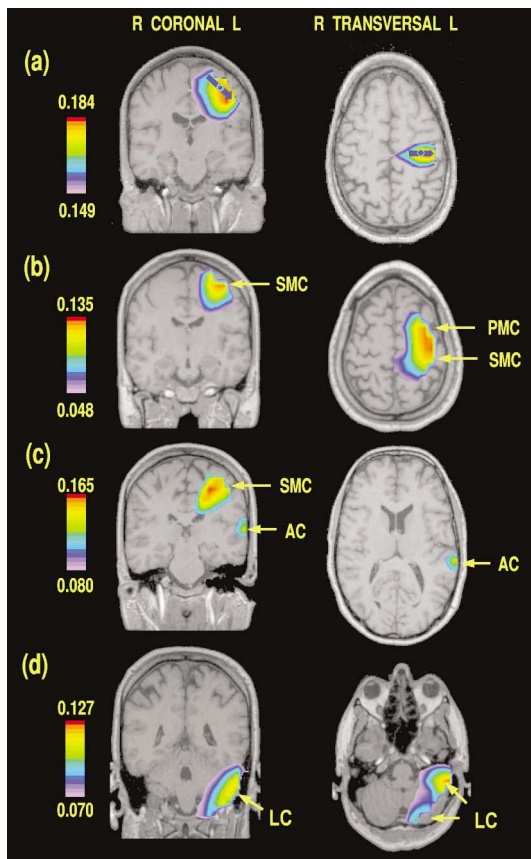

FIG. 2 (color). (a) Simulation: A simulated current with time course ξ_1 and fixed orientation and location $\mathbf{x}_0$ (“→”) in the left sensorimotor cortex (SMC) of a real brain generates a magnetic field. $\mathbf{x}_0$ is reliably detected with the 1:1 synchronization index (1) between ξ_1 and all voxels [15]. (b)–(d) Experiment: Synchronization indices $\rho_{1,2}$ [16] between the EMG of the right flexor digitorum muscle (RFM) (2-Hz band) and brain currents (4-Hz band) [(b),(c) during first minute], and $\rho_{1,1}$ between RFM (2-Hz band) and brain currents (2-Hz band) [(d), during second minute]; window length $T = 60$ s. Areas with local maxima of $\rho_{1,2}$ and $\rho_{1,1}$ are shown in corresponding coronal and transversal brain sections: left secondary auditory cortex (AC), left cerebellum (LC), left premotor cortex (PMC), and left SMC [14].
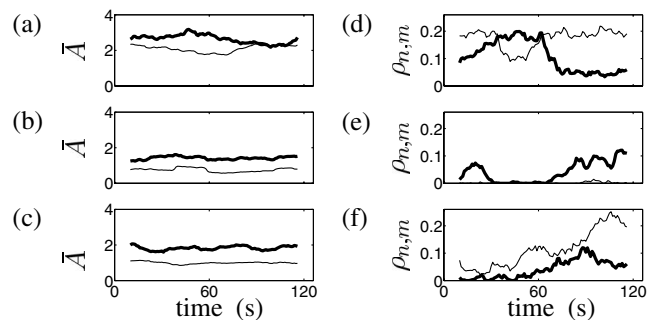

FIG. 3. (a)–(c): Averaged amplitudes $\bar{A}$ of the current source density from (3) in arbitrary units of the 2-Hz band (1–3 Hz, bold line) and the 4-Hz band (3–5 Hz, thin line) of SMC (a), of LC (b), and of AC (c). $\bar{A}$ of PMC is similar to $\bar{A}$ of AC. Brain/muscle synchronization (CMS) in (d),(e): CMS between RFM and SMC (d), RFM and LC (e). Synchronization index $\rho_{1,1}$ [16] for the 2-Hz band of both muscle activity and brain currents (bold) and $\rho_{2,1}$ for 2-Hz band of muscle activity and 4-Hz band of brain currents (thin). 1:1 brain/brain synchronization (CCS) between SMC and PMC (f): $\rho_{1,1}$ for the 2-Hz band (bold) and for the 4-Hz band (thin) of the currents of both areas. No 2:1 CCS within or between brain areas was found. (a)–(f) Window length $T = 20$ s [14].

and 1:2 CMS [Fig. 3(d)]. (c) Coherence cannot distinguish between amplitude and phase dynamics (Fig. 3).

Remarkably, the activity, i.e., the averaged amplitude $\bar{A}(\mathbf{x}, t)$ of the cerebral currents, hardly changes during the experiment in all relevant brain areas [Fig. 3(a)–3(c)]. Not the activity of brain areas associated with movement coordination, inner voice, and time estimation, but their phase synchronization behavior is related to internal rhythm generation. The latter, though crucial with regard to the biological question at hand, would escape detection with fMRI or positron emission tomography (assessing brain metabolism or neurotransmitter distribution) and, thus, demonstrates the important functional insight that can be gained with our novel method. In addition, our method may also be applied to study the spatiotemporal spread of excitation in the heart and, particularly relevant for cardiac arrhythmias, the synchronization of pathological reentry processes which can be detected with magnetocardiography (but not with electrocardiography).

[1] R. L. Stratonovich, *Topics in the Theory of Random Noise* (Gordon and Breach, New York, 1963).

[2] Y. Kuramoto, *Chemical Oscillations, Waves, and Turbulence* (Springer, Berlin, 1984).

[3] M. G. Rosenblum *et al.*, Phys. Rev. Lett. **76**, 1804 (1996).

[4] R. Rozenfeld *et al.*, Phys. Rev. E **64**, 051107 (2001).

[5] P. Tass *et al.*, Phys. Rev. Lett. **81**, 3291 (1998).

[6] A. Neiman *et al.*, Phys. Rev. Lett. **83**, 4896 (1999).

[7] E. von Holst, Erg. Physiol. **42**, 228 (1939).

[8] The magnetic field is registered with a whole-head magnetometer system (Magnes 2500 WH, 4D-Neuroimaging) with 148 SQUIDs (sensors). With magnetic field tomography (MFT) [A. A. Ioannides *et al.*, Inverse Probl. **6**, 523 (1990)] we determine the cerebral current source density $\mathbf{j}(\mathbf{x}, t)$ in a single run mode, for each time t separately, on a supercomputer (Cray T3E): The jth sensor measures the signal $m_j(t) = \int_Q d^3 x f_j(\mathbf{x}) \mathbf{j}(\mathbf{x}, t)$, where $f_j(\mathbf{x})$ is the sensitivity profile of the jth sensor, and Q is the source space (a spheric segment fitted to a hemisphere of the brain). $\mathbf{j}(\mathbf{x}, t) = \sum_{j=1}^{M} a_j(t) f_j(\mathbf{x}) w(\mathbf{x})$, where the sum runs over all sensors, and $a_1(t), \dots, a_M(t)$ have to be determined. $w(\mathbf{x})$ is an exponential weight function decreasing from the center to the surface of the brain. For each individual brain $w(\mathbf{x})$ is calibrated with simulated data to achieve an optimal spatial resolution for both superficial and deep cerebral currents. We get $m_j(t) = \sum_{k=1}^{M} P_{jk} a_k(t)$, where $P_{jk} = \int_Q d^3 x f_j(\mathbf{x}) f_k(\mathbf{x}) w(\mathbf{x})$. A stable regularization technique yields $a_k(t)$. The spatial resolution is improved with one iteration, where $w(\mathbf{x}) \rightarrow w(\mathbf{x}) |\mathbf{j}(\mathbf{x}, t)|$. We apply MFT to the left and right hemispheres separately.

[9] A. M. Wing and A. B. Kristofferson, Percept. Psychophys. **14**, 5 (1973).

[10] R. B. Ivry *et al.*, Exp. Brain Res. **73**, 167 (1988).

[11] M. A. Pastor *et al.*, Brain **115**, 875 (1992).

[12] S. M. Rao *et al.*, J. Neurosci. **17**, 5528 (1997).

[13] P. Panter, *Modulation, Noise, and Spectral Analysis* (McGraw-Hill, New York, 1965); R. K. Otnes and L. Enochson, *Digital Time Series Analysis* (John Wiley & Sons, New York, 1972); S. L. Marple, *Digital Spectral Analysis* (Prentice-Hall, Englewood Cliffs, NJ, 1987).

[14] Our results are robust with respect to variations (i) of the edges of the FIRCLS bandpass filters [I. W. Selesnick, M. Lang, and C. S. Burrus, IEEE Trans. Signal Process. **44**, 8 (1996)] of ± 0.5 Hz and (ii) of the window length T between 15 and 60 s. For the 2-Hz band and the 4-Hz band, completely independent signals with the same spectral bandwidth give a diffusion of their instantaneous phase difference of approximately 2 rad/s. This indicates that spurious synchronization can be avoided as long as the window length T is greater than 15 s. Our findings were additionally confirmed by analyzing the signals filtered with broader bands (e.g., 1–5 Hz). n and m of $\Psi_{n,m}$ were chosen according to the prominent peaks in the spectra (Fig. 1). PMC and SMC are joined in Fig. 2(a), but can be separated by taking into account the averaged amplitude $\bar{A}$ from (3): $\bar{A}$ is high in both areas and low in between. Similar results as in Figs. 2 and 3 are obtained with the right extensor indices muscle as reference. Large amplitude $\bar{A}$ from (3) corresponds to high changes in blood oxygenation level found with fMRI [12].

[15] To simulate a brain rhythm we use the Rössler system $\dot{\xi}_1 = -\omega \xi_2 - \xi_3 + \mu$, $\dot{\xi}_2 = \omega \xi_1 + 0.15 \xi_2$, $\dot{\xi}_3 = 0.2 + \xi_3 (\xi_1 - 10)$, with $\omega = 1$, Gaussian white noise, $\langle \mu(t) \mu(t') \rangle = 2 \delta(t - t')$, and Euler's technique with time step $\Delta t = 2\pi/1000$ (see [5]).

[16] $\rho_{n,m}[s(t), \mathbf{j}(\mathbf{x}, t)] = \max_{k=1}^{3} \max \{ \tilde{\rho}_{n,m}[s(t), j_k(\mathbf{x}, t)] - \rho_{n,m}^{A}, 0 \}$ belongs as significant synchronization index to (1) and $\rho_{n,m}[\mathbf{j}(\mathbf{x}_1, t), \mathbf{j}(\mathbf{x}_2, t)] = \max_{k,l=1}^{3} \max \{ \tilde{\rho}_{n,m}[j_l(\mathbf{x}_1, t), j_k(\mathbf{x}_2, t)] - \rho_{n,m}^{B}, 0 \}$ to (2).

[17] The 1:2 CMS might be due to two antiphase synchronized neuronal populations which activate flexor and extensor muscle alternatingly, as also observed in Parkinsonian tremor [5]. Because of the limited spatial resolution of MEG, MFT reconstructs a 4-Hz oscillation which is a superposition of two 2-Hz oscillations originating from nonseparable sources.

[18] J. Pich, Span. J. Psychol. **3**, 63 (2000).

[19] Each MEG sensor measures signals s_j originating from more than one brain area, so that MEG signals are linear superpositions of s_j. A simple model of MEG signals picked up over remote sources is $a = (1 - \varepsilon) s_1 + \varepsilon s_2$ and $b = \varepsilon s_1 + (1 - \varepsilon) s_2$ with small and positive ε, where s_1 and s_2 are the signals originating from these sources. a and b are significantly coherent even if s_1 and s_2 and, thus, also a and b are not phase synchronized [5]. This leads to a spatial overestimation of synchronized MEG channels, when coherence is applied [5]. Analogously, the linear superposition effect applies to the reconstructed cerebral current source density $\mathbf{j}(\mathbf{x}, t)$.